# Lawrence Berkeley National Laboratory

## LBL Publications

### Title

Optical constants of magnetron sputtered aluminum in the range 17—1300 eV with improved accuracy and ultrahigh resolution in the L absorption edge region

### Permalink

https://escholarship.org/uc/item/42q6h3gj

### Journal

Journal of Applied Physics, 136(19)

### ISSN

0021-8979

### Authors

Burcklen, Catherine
Delmotte, Franck
Alameda, Jennifer
et al.

### Publication Date

2024-11-21

### DOI

10.1063/5.0233781

### Copyright Information

This work is made available under the terms of a Creative Commons Attribution License, available at https://creativecommons.org/licenses/by/4.0/

Peer reviewed

eScholarship.org Powered by the California Digital Library
University of California

Journal of Applied Physics

RESEARCH ARTICLE | NOVEMBER 20 2024

# Optical constants of magnetron sputtered aluminum in the range 17–1300 eV with improved accuracy and ultrahigh resolution in the L absorption edge region

Catherine Burcklen ; Franck Delmotte ; Jennifer Alameda; Farhad Salmassi; Eric Gullikson ; Regina Soufli

*J. Appl. Phys.* 136, 195106 (2024)
https://doi.org/10.1063/5.0233781

View Online
Export Citation

Articles You May Be Interested In

Soft x-ray optical constants of sputtered chromium thin films with improved accuracy in the L and M absorption edge regions
*J. Appl. Phys.* (July 2018)

Effect of surface oxidation on soft x-ray optical properties of ion beam sputter deposited amorphous AlN thin film
*J. Appl. Phys.* (November 2021)

$Cr/B_4C$ multilayer mirrors: Study of interfaces and X-ray reflectance
*J. Appl. Phys.* (March 2016)

10 December 2024 22:19:30

Journal of
Applied Physics

ARTICLE

pubs.aip.org/aip/jap

# Optical constants of magnetron sputtered aluminum in the range 17–1300 eV with improved accuracy and ultrahigh resolution in the L absorption edge region

Cite as: J. Appl. Phys. **136**, 195106 (2024); doi: 10.1063/5.0233781
Submitted: 17 August 2024 · Accepted: 5 November 2024 ·
Published Online: 20 November 2024

Catherine Burcklen,[1,a)] Franck Delmotte,[2] Jennifer Alameda,[1] Farhad Salmassi,[3] Eric Gullikson,[3] and Regina Soufli[1]

## AFFILIATIONS

[1]Lawrence Livermore National Laboratory, 7000 East Avenue, Livermore, California 94550, USA
[2]Université Paris-Saclay, Institut d'Optique Graduate School, CNRS, Laboratoire Charles Fabry, 91127, Palaiseau, France
[3]Lawrence Berkeley National Laboratory, 1 Cyclotron Rd., Berkeley, California 94720, USA

[a)]**Author to whom correspondence should be addressed:** burcklen1@llnl.gov

10 December 2024 22:19:30

## ABSTRACT

This work determines a new set of EUV/x-ray optical constants for aluminum (Al), one of the most important materials in science and technology. Absolute photoabsorption (transmittance) measurements in the 17–1300 eV spectral range were performed on freestanding Al films protected by carbon (C) layers, to prevent oxidation. The dispersive portion of the refractive index was obtained via the Kramers–Kronig transformation. Our data provide significant improvements in accuracy compared to previously tabulated values and reveal fine structure in the Al $L_1$ and $L_{2,3}$ regions, with photon energy step sizes as small as 0.02 eV. The implications of this work in the successful realization of EUV/x-ray instruments and in the validation of atomic and molecular physics models are also discussed.

*© 2024 Author(s). All article content, except where otherwise noted, is licensed under a Creative Commons Attribution-NonCommercial-NoDerivs 4.0 International (CC BY-NC-ND) license (https://creativecommons.org/licenses/by-nc-nd/4.0/).* https://doi.org/10.1063/5.0233781

## I. INTRODUCTION

Aluminum (Al) is an essential material for instrumentation at short wavelengths, including the ultraviolet (UV), extreme ultraviolet (EUV), and x-ray ranges. Applications that reside in these spectral regions include attosecond physics/ultrafast science, coherent sources including synchrotrons and free-electron lasers, plasma physics, solar physics and astrophysics, and semiconductor photolithography, a trillion-dollar industry. These applications require optics systems composed of increasingly complex thin film structures that demand accurate knowledge of the optical properties (refractive indices) of their constituent materials, in order to build realistic models that accurately predict the optical system performance. In the EUV/x-ray region, Al is the most commonly used transmissive filter material.[1] Al is also a component of reflective (mirror) and diffractive (grating) coatings, including narrowband or broadband multilayer interference coatings[2] such as Al/Zr,[3] AlMg/SiC,[4,5] Al/Sc,[6,7] Al/Mo/SiC,[8–10] Al/Mo/B4C,[11] Al/Sc/SiC,[6,7] Mo/Al/Sc,[6,7] and Al/$Y_2O_3$.[12]

In the EUV and x-ray spectral range, the photon energy-dependent refractive index of materials can be written as

$$n = 1 - \delta + i\beta, \tag{1}$$

where $\delta$ and $\beta$ are known as the optical constants of the material.

The EUV/x-ray optical constants of Al have been measured by a variety of techniques over the past 60 years. These include the determination of $\beta$ via photoabsorption (transmittance) measurements combined with a Kramers–Kronig analysis for the determination of $\delta$,[13–15] fitting both $\delta$ and $\beta$ from reflectance[16–18] or electron-energy-loss[19] measurements, as well as interferometry.[20] Rakić[21] have also presented an algorithmic approach toward the determination of $\delta$ and $\beta$ for Al in a wide range of the spectrum,



© Author(s) 2024

via a combination of models and Kramers–Kronig analysis, using experimental data available from the literature at the time. The Atomic Data Tables website owned by the Center for X-ray Optics (CXRO) at LBNL[22,23] maintains the definitive database for the optical constants of all materials in the 30 eV–30 keV spectral range, using a compilation of existing experimental data interpolated with a model based on the single-atom approximation for $\beta$, and the Kramers–Kronig transformation for $\delta$.

Despite the wealth of experimental data and being recognized as one of the materials whose optical properties are among the most studied, the existing optical constants for Al are still vastly inaccurate in the region of the $L_1$ and $L_{2,3}$ edges and in the low-energy portion of the EUV spectral range.[24,25] The optical constants of Al were identified as a major source of uncertainty toward predicting the performance of Al-based optics,[25] including Al filters widely employed in EUV/x-ray instrumentation, from synchrotron and laser sources to space telescopes for solar physics and space weather monitoring. The lack of accurate refractive index values for such an important material is a problem that is not unique to Al[25] and can be explained by the difficulties in performing measurements in the EUV/x-ray spectral region, as discussed in the next paragraph. Additionally, and although sophisticated atomic physics models have been developed for the calculation of the optical properties of materials, to date these models cannot provide adequately accurate values for thin film materials. This is especially true in the vicinity of absorption edges and at lower photon energies, where inter-atomic effects and other associated properties such as the morphology (crystallinity) of the film (which may also depend on the deposition technique) can affect the optical constants of the thin film material.

The EUV/x-ray spectral range poses serious challenges to optical constant measurement techniques. Reflectance, interferometry, and ellipsometry-based methods provide experimentally both $\delta$ and $\beta$ values of the material under study. However, these methods are extremely sensitive to surface microroughness, as well as to contamination and oxidation layers present in the samples under study, even at the atomic monolayer level. A model of the measured samples needs to be built that includes these effects as parameters and fitting processes need to be deployed that suffer from non-uniqueness solution issues.[26–28] Performing measurements *in situ*, immediately after deposition of the samples (i.e., under vacuum), may partially alleviate some of these issues, but it is experimentally complicated.[17,18,29] Also very importantly, the fitting process for ($\delta$, $\beta$) becomes most challenging in the vicinity of absorption edges. This is due to abrupt changes in $\delta$ and $\beta$ values and to the relationship between $\delta$ and $\beta$ in these spectral regions.[26,30–32] Finally, reflectance requires a separate set of data vs incidence angle followed by a fitting process for each photon energy, making it time-consuming to produce ($\delta$, $\beta$) values over large spectral regions. Ultimately, the selection of the most suitable measurement technique for a given material may depend on the spectral region of interest as well as on specific properties of the material under study.

Earlier work[33–39] established a transmittance (photoabsorption)-based methodology as a very reliable technique for the determination of the optical constants in the soft x-ray/EUV, as it overcomes most of the difficulties specific to this spectral range, including the sensitivity to roughness and to the presence of oxidation and contamination layers, discussed in the previous paragraph. The transmittance $T$ through a thin film sample is given by the equation

$$T(\lambda) = T_0(\lambda)\exp(-4\pi\beta(\lambda)d/\lambda), \tag{2}$$

where $d$ is the layer thickness of the material under study, $\lambda$ is the photon wavelength (related to the photon energy $E$ by $E = hc/\lambda$), and $T_0$ is the transmittance of other layers that may be present on the sample. $T_0$ can be normalized out of the data, which makes this technique attractive, as will be discussed later in this paper. Very importantly, this technique allows a straightforward determination of photoabsorption ($\beta$) values over wide spectral ranges with exquisite resolution near absorption edges. To employ and fully take advantage of this technique, one would require (i) the ability to fabricate freestanding thin films of different thicknesses of the material under study and (ii) access to a well-calibrated, monochromatic, tunable EUV/x-ray facility equipped with control software that allows fast, precise, and reproducible scans of photon energy. Such capabilities enabled the present work and will be discussed in detail in this paper. The values of $\delta$ can then be determined from $\beta$ via the Kramers–Kronig transformation.

It should be noted that Eq. (2) is valid only in the case where there are no internal reflections between the layers of the sample under study. At the lower EUV photon energies, the optical contrast between the layers increases and allows the presence of significant multiple reflections inside the films, rendering Eq. (2) invalid.[40] For most materials, the photon energy where multiple reflections start becoming significant is around 62 eV. A new method was recently developed that overcomes the issue of multiple reflections in transmittance data and was employed to determine the photoabsorption $\beta$ of Al in the photon energy range 17–62 eV.[40]

This paper presents a new determination of the optical constants of Al in the range 17–1300 eV via transmittance measurements through a series of freestanding thin films. The new photoabsorption data were combined with existing data from the literature in other spectral regions (including the recent data from Ref. 40 discussed in the previous paragraph) to create via the Kramers–Kronig analysis a new set of optical constants ($\delta$, $\beta$) for Al in an extended spectral range (17–1300 eV), with improved accuracy and ultrahigh resolution in the Al $L_1$ and $L_{2,3}$ edge regions. Finally, the new set of optical constants was validated with the simulation of the performance of Al-based filters and the comparison with previous experimental data.

## II. EXPERIMENTAL SETUP

### A. Thin film deposition

C/Al/C films with different Al thicknesses were deposited at LLNL by Direct Current (DC) magnetron sputtering, using a planar deposition system where each substrate is mounted on a deposition platter that is rotating above the sputtering sources. Each C/Al/C sample intended for transmittance measurements was deposited on a photoresist-coated Si wafer substrate and was accompanied by a second, identical C/Al/C sample deposited on a bare Si substrate, with both samples deposited during the same deposition run. The second C/Al/C sample was intended to be

10 December 2024 22:19:30



© Author(s) 2024

used as a "witness" for characterizations, as will be discussed in Sec. III. The Si wafer substrates have (100) Si crystal orientation, 100 mm diameter and 525–550 $\mu$m thickness and a surface micro-roughness in the range 0.1–0.2 nm root-mean-square (RMS). Rectangular sputtering sources with $127 \times 254$ cm$^2$ dimensions and purity better than 99.99% were used for both Al and C depositions, operated at a constant power of 200 W. The base vacuum pressure in the deposition system was on the order of $10^{-7}$ Torr and the Ar process gas pressure was 1 mTorr. All deposition parameters (including the rotation velocities of the deposition platter during C and Al deposition) were identical among all deposition runs, except for the number of platter revolutions during Al deposition, which was changed in each run to achieve a different Al thickness (see also Sec. III).

### B. GIXR

C/Al/C witness samples were characterized by means of grazing incidence x-ray reflectometry (GIXR) (reflectance vs incidence angle measurements) using a Panalytical Xpert Pro MRD$^{TM}$ instrument at LLNL, equipped with a Cu K$_\alpha$ anode source, which emits x rays at 8.05 keV photon energy, a W/Si-coated Goebel mirror, and a Ge monochromator.

### C. RBS

Rutherford Backscattering (RBS) measurements with 2.275 MeV He$^{++}$ ions and a backscattering angle of 160° were performed at EAG Eurofins Labs (Sunnyvale, California).

### D. EUV/soft x-ray transmittance

The EUV/soft x-ray transmittance measurements discussed in this paper were performed at beamline 6.3.2 of the Advanced Light Source (ALS) synchrotron, operated by the CXRO at LBNL. Beamline 6.3.2 has a grating monochromator with a fixed exit slit and its general characteristics have been described in detail earlier.[41,42] Three monochromator gratings (80, 200, and 1200 lines/mm) were used to access the photon energy range 17–1300 eV. The beam size is 100 $\mu$m in the horizontal direction; the vertical beam size is determined by the exit slit and was set at 60 $\mu$m throughout the transmittance vs photon energy measurements. In the region of the Al L$_{2,3}$ edge (72–75 eV) the spectral resolving power ($E/\Delta E$) of the beamline, using the 200 lines/mm grating, is estimated at around 2000.[43] In order to fully resolve the near-edge fine structure, data were collected with an exceptionally small step size of 0.02 eV (see also Sec. IV). The capability of the beamline monochromator to move accurately and reproducibly in such small steps, combined with the beamline resolving power, enabled the ultrahigh-resolution of the data presented in this work. In the rest of the photon energy range, measurements were taken in steps ranging from 0.1 to 6 eV, with the finer steps used in spectral ranges where fine structure was present. Photon energy calibration was based on the absorption edges of a series of transmission filters (Al, Si, Ti, Cr) with a relative accuracy of 0.011% rms and could be determined with 0.007% repeatability. For second harmonic and stray light suppression, a series of transmission filters (Mg, Al, Si, Be, Zr, C, Ti, Cr, Co, Cu) was used. For higher-order harmonic suppression, an "order suppressor" consisting of three C or Ni mirrors at a variable grazing incidence angle (20° to 6°, depending on photon energy range) and based on the principle of total external reflection, is used in addition to the filters. The measurement chamber allows translation of the sample in three dimensions, tilt in two dimensions and azimuth rotation of the sample holder. The available detectors include various photodiodes and a CCD camera (the latter for sample alignment), which can be rotated by 360° around the axis of the chamber. During the measurements discussed in this paper, signal was collected with a Si photodiode detector with a 10–10 mm$^2$ active area and acceptance angle of 2.4°. The ALS storage ring current was used to normalize the signal against the storage ring current decay. The base pressure in the measurement chamber was $10^{-7}$ Torr.

10 December 2024 22:19:30

## III. SAMPLE PREPARATION AND CHARACTERIZATION

The five thinnest witness samples, consisting of a C/Al/C stack deposited on a Si wafer, were measured by GIXR in order to determine the Al and C layer thicknesses. The results are summarized in Table I. Figure 1(a) shows the GIXR data for the 90 and the 45.6 nm-thick Al samples, together with their simulated curves. In the simulations, we adjusted the Al and C layer thicknesses and surface roughnesses to fit the high- and low-frequency Kiessig fringes in the GIXR data (which depend on the Al and C layer

**TABLE I.** List of samples and their parameters obtained from the fit to the GIXR data. The asterisk* shows samples for which the thickness was extrapolated as shown in Fig. 1(b).

| Sample | Bottom C thickness (nm) | Al layer | | | Top C thickness (nm) |
|---|---|---|---|---|---|
| | | Number of revolutions | Fitted thickness (nm) | Al top roughness (nm rms) | |
| M1-200224A1 | 5.5 | 5 | 22.4 | 2.3 | 5.5 |
| M1-200224B1 | 5.5 | 10 | 45.6 | 2.7 | 5.5 |
| M1-200225A1 | 5.5 | 20 | 90 | 1.7 | 5.5 |
| M1-200226A1 | 5.5 | 30 | 137.5 | 3.0 | 5.5 |
| M1-200226B1 | 5.5 | 40 | 185 | 3.0 | 5.5 |
| M1-200225B1 | 5.5 | 60 | 277* | N/A | 5.5 |
| M1-200227A1 | 5.5 | 80 | 369.7* | N/A | 5.5 |


© Author(s) 2024

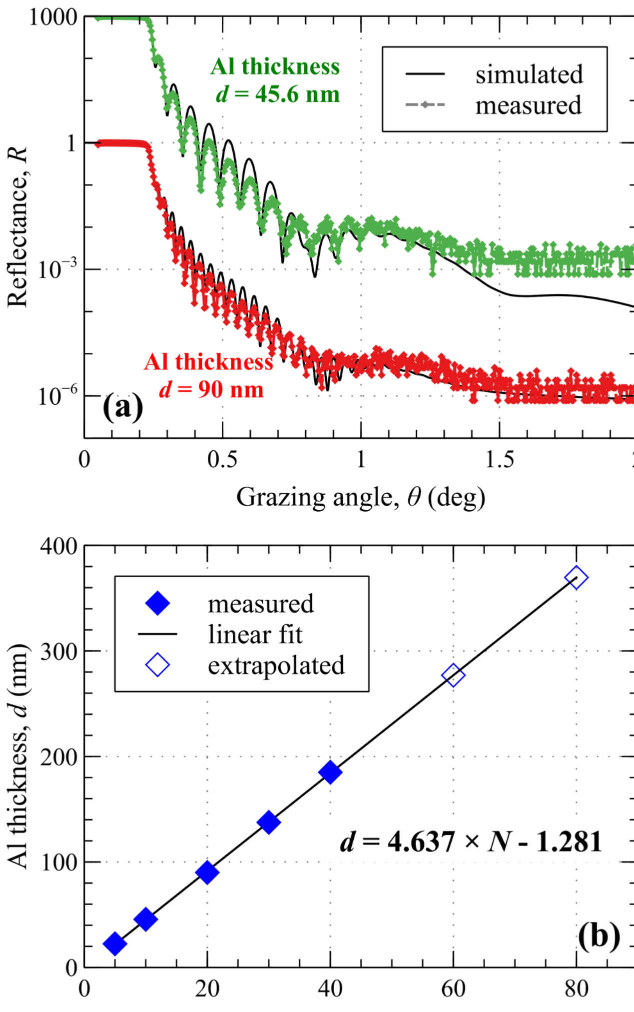


**FIG. 1.** (a) GIXR data of two C/Al/C films deposited on a Si wafer. The measured data are shown in green and red dots and the simulated curves are shown as black solid lines. The thicknesses of the Al layers, simulated to fit the GIXR data, are 45.6 nm (green) and 90 nm (red), and the C layers are 5.5 nm thick each. The plots from the 45.6 nm thick Al film have been shifted on the y-axis, for better visibility. (b) Measured Al thickness (blue filled diamonds) and linear fit (black line) as a function of the number of platter revolutions. The Al thicknesses were obtained by fitting the GIXR data, as illustrated in (a). The linear fit was used to extrapolate the thickness values for the two thickest films (blue unfilled diamonds).

thicknesses, respectively). Tabulated atomic scattering factor values and the bulk Al density value were used for the optical constants of Al. Tabulated atomic scattering factors with a density of 1.95 g/cm$^3$ were used for the optical constants of C. The density of the C layers was determined by fitting the position of the critical angle in the GIXR data of C single films deposited as part of the calibration of the C layer thickness. The substrate in the simulations was Si and we used a 0.6 nm thick $SiO_2$ layer between the substrate and the first C layer to simulate the native oxide on top of the Si wafer. The roughness of both the substrate and the $SiO_2$ layer was set to 0.2 nm rms. We obtained a good agreement between the experimental and simulated critical angle for all C/Al/C samples (see, for example, Fig. 1). This confirms that the density of the Al thin films used in this study is very close to the nominal bulk density (2.7 g/cm$^3$) used in the tabulated optical constants.[22,23]

In this manner, we were able to determine the Al thickness for the five thinnest samples (22.4, 45.6, 90, 137.5, and 185 nm) and we also determined an equation for the Al thickness vs number of platter revolutions, displayed in Fig. 1(b). For the two thickest samples (60 and 80 revolutions), the Kiessig interference patterns in the GIXR data were too weak to obtain a reliable fit for the Al layer thickness. Because the number of platter revolutions was the only parameter that was changed between different Al deposition runs to achieve a specific Al thickness (see also Sec. II), we used the equation in Fig. 1(b) to determine the thickness of the two thickest Al films. We obtained similar interfacial roughness/interdiffusion values (between 0.5 and 1 nm rms at the C/Al interface below the Al layer and between 1.7 and 3.2 nm rms above the Al layer) for all samples, as shown in Table I. Moreover, we determined the same thickness value for all the C layers (5.5 nm) in all five C/Al/C samples measured by GIXR. The C and Al thickness values determined in this manner have an estimated accuracy better than 1%.

RBS measurements on one thin sample (22.4 nm) and one thick sample (185 nm) revealed that the Al layers are more than 99.9% pure and that the C layers are 99.7% pure. 0.3% (atomic) of Ar was detected in the C layers, presumably from the Ar process gas during deposition.

The C/Al/C films were removed from their substrates and mounted as freestanding films at CXRO/LBNL, using a method that has also been discussed earlier.[38] Briefly, to produce freestanding C/Al/C films, washers (with each washer having a 3-mm-diameter aperture) were glued on the C/Al/C films that were deposited on photoresist-coated Si wafers, followed by removal of the photoresist by chemical etching. The freestanding C/Al/C films remained attached to the washers after photoresist removal, which allows easy handling of the freestanding samples. Then, the freestanding C/Al/C films were cleaned of resist residues by exposure under a UV-ozone lamp in air. Several freestanding C/Al/C samples with 45.6 nm-thick Al were used in order to optimize the UV-ozone cleaning process. Figure 2(a) shows the evolution of the sample transmittance at 70.85 eV photon energy over the 3 mm washer aperture, as a function of the UV-ozone exposure time. One can note that it takes about 130 min to reach the maximum transmittance. Yet, when increasing the exposure time, the uniformity of transmittance over the sample aperture continues to improve and the best results are obtained after a total exposure time of 228 min. This procedure has been also applied in earlier work,[33,37–39] however, the optimal UV-ozone exposure time estimated in this study is significantly longer than in previous studies.[26,38] This is because the photoresist used in the previous studies was different. Figure 2(b) shows the transmittance measured at 70.85 eV for the five C/Al/C freestanding samples used in transmittance vs photon energy measurements to determine Al photoabsorption (see Sec. IV), after 228 min of UV-ozone exposure. The uniformity over the sample

10 December 2024 22:19:30


© Author(s) 2024

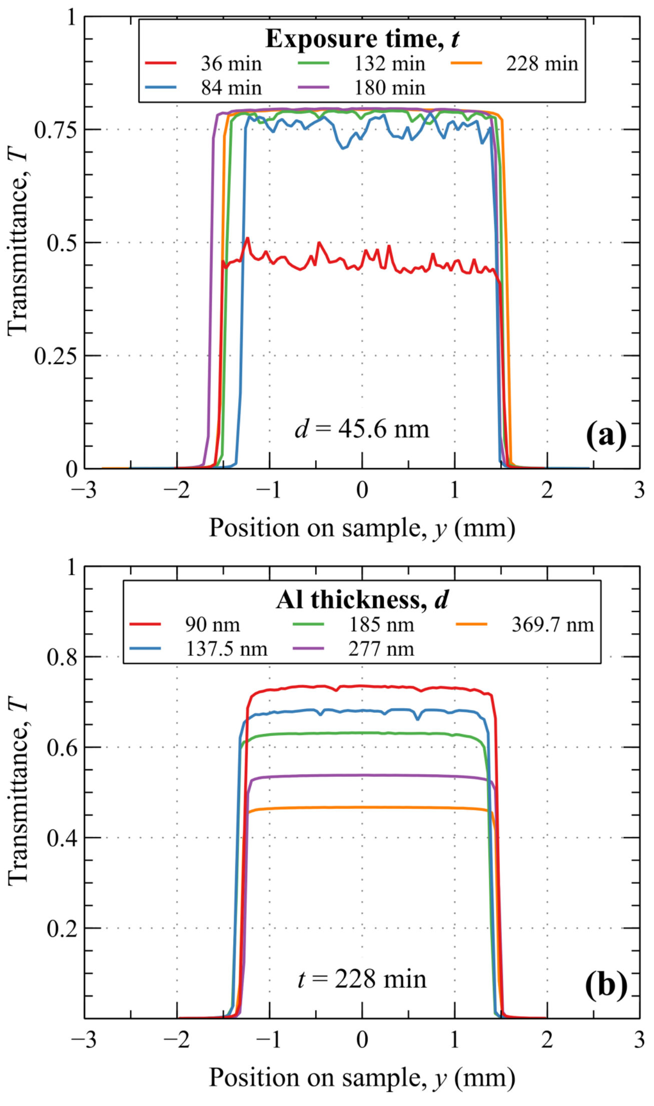


**FIG. 2.** Measured transmittance at 70.85 eV, as a function of the vertical position on the sample, on (a) a C/Al/C film with an Al thickness of 45.6 nm, for various exposure times to the UV-ozone lamp, and (b) all C/Al/C samples used in the present study (with the Al thickness shown in the legend), with an exposure time of 228 min.

aperture is better than 0.6% RMS. Prior to the measurement of each transmittance spectrum, each sample was aligned to set the beam on the center of the aperture with an accuracy of $\pm 0.1$ mm. In that range, the error in transmittance due to sample non-uniformity is less than 0.3% (relative).

We note that the two thinnest Al films shown in Table I (22.5 and 45.6 nm thick) were used for thickness calibrations (including GIXR measurements), and various tests post UV-ozone exposure [see, for example, Fig. 2(a)]. They were also used to verify the purity of the films against contaminants such as oxygen and photoresist residue, via transmittance measurements (not shown here) around the carbon and oxygen K edge spectral regions (see also Ref. 38). It is interesting to notice that any hypothetical photoresist residues would not affect the determination of Al photoabsorption, as long as they are of the same thickness on all samples. Indeed, their signal would be normalized out, as is the case for the C capping layers.

## IV. DETERMINATION OF Al OPTICAL CONSTANTS: RESULTS AND DISCUSSION

The transmittance curves in Figs. 3 and 4 were obtained through the expression $T = I/I_0$ for the transmittance $T$ of a film

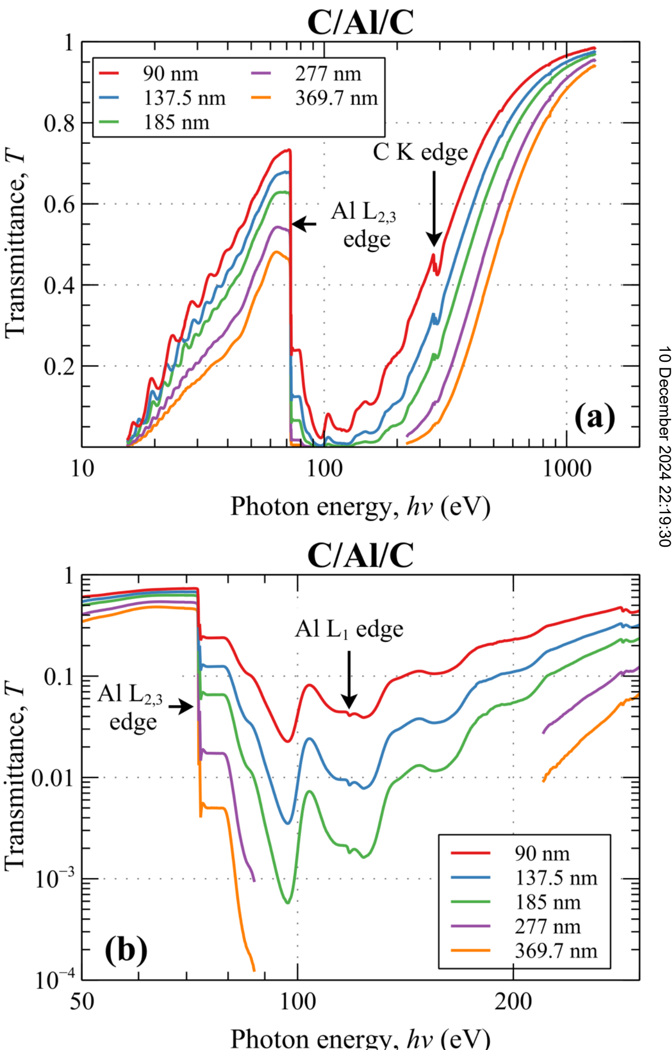


**FIG. 3.** Experimental transmittance vs photon energy spectra for all C/Al/C samples: (a) log-lin plot, (b) log-log plot focused in the photon energy range 50–300 eV.

10 December 2024 22:19:30


© Author(s) 2024

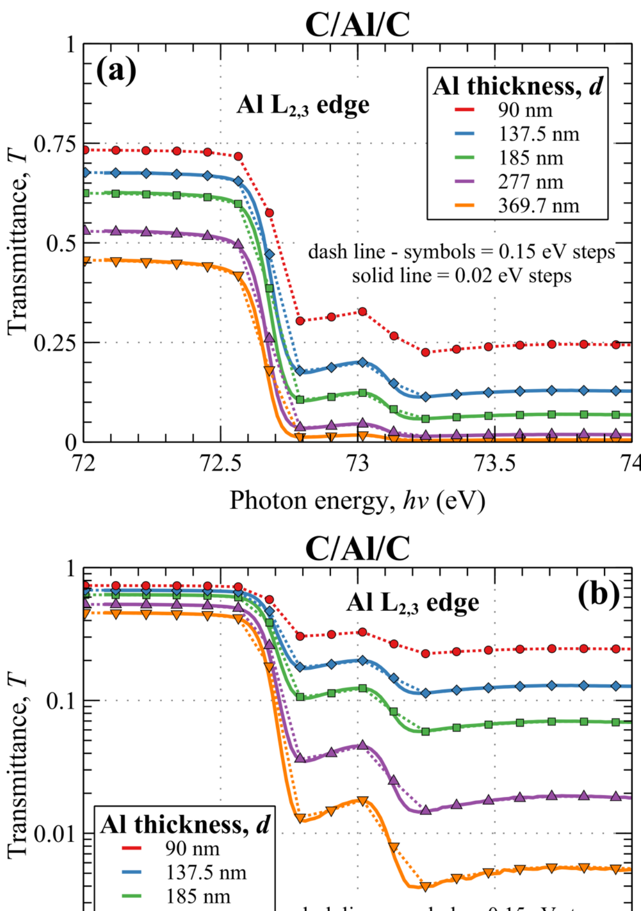


**FIG. 4.** Experimental transmittance vs photon energy spectra for C/Al/C samples in the vicinity of the Al $L_{2,3}$ edge: (a) lin-lin plot and (b) lin-log plot. Measurements with larger photon energy step size (0.15 eV steps) were performed initially and are shown as a dashed line and symbols. Measurements with ultra-low step size (0.02 eV steps) were performed later and are shown as a solid line.

at a given photon energy, where $I$ is the intensity transmitted through the film and $I_0$ is the intensity of the incident photon beam. Figure 3 shows transmittance vs photon energy measurement results on five free-standing C/Al/C samples with Al thicknesses ranging from 90 to 369.7 nm. Figure 3(a) shows the entire spectral range of the measurements, 17–1300 eV. At the lowest photon energies (17–62 eV), multiple reflections among the C/Al/C layers result in oscillations of the transmittance data, as is evidenced in Fig. 3(a). Therefore, as is also discussed in Sec. I, Eq. (2) is not valid in the spectral region 17–62 eV. A new methodology was developed in Ref. 40 for transmittance data with oscillations and it was applied to determine the photoabsorption ($\beta$) for Al in the spectral range 17–62 eV; these values are employed later in this section. Figure 3(a) includes the aluminum L and carbon K edge spectral regions and Fig. 3(b) shows the Al $L_1$ and $L_{2,3}$ edge regions and their fine structure in detail, with the transmittance plotted on a logarithmic axis. Transmittance values over four orders of magnitude are shown; the two C/Al/C samples with the thickest Al layers (277 and 367.9 nm) produced transmittance data points with increased noise in the energy range above the Al $L_{2,3}$ edge. This was due to (i) transmittance values below 0.001, or (ii) transmittance values between 0.01 and 0.001, in a spectral region with decreased incident photon flux. These spectral regions with "noisy" data from the two thickest Al films were not included in the plots of Fig. 3 or in the data analysis. In Fig. 3(b), a feature attributed to the Al $L_1$ edge, consisting of a pointed "dip" at 118.08 eV surrounded by other fine structure, is revealed for the first time in the literature. It should be noted that the transmittance measurements in the photon energy region (50–111.7 eV) which includes the Al $L_1$ and $L_{2,3}$ edges were obtained in steps of 0.15 eV, which were considered small enough to resolve all the near-edge fine structure, as shown in Fig. 3. However, closer observation during data analysis revealed that the fine structure right at the Al $L_{2,3}$ edge was still not fully resolved. This is illustrated in Fig. 4, which shows transmittance vs photon energy measurements in the spectral region 72–74 eV, obtained with 0.15 and 0.02 eV steps. The latter are ultrahigh-resolution measurements that push the limits of modern instrumentation and demonstrate the capability of beamline 6.3.2 and of the methodology applied in this paper, to resolve the finest, previously un-seen features in near edge absorption fine structure (NEXAFS) or x-ray absorption near edge structure (XANES) of materials. It should also be noted that the 0.02 eV-step measurements were obtained 2 years after the 0.15 eV-step measurements, with the samples having been stored in air, in a clean cabinet located by the beamline. The overlap between the two sets of measurements in Fig. 4 is remarkable, especially if one considers that the spectral region of the Al $L_{2,3}$ edge would be the most sensitive to any compositional changes in the measured Al films. This means that the freestanding C/Al/C samples remained extremely stable over a period of 2 years, with the Al layers fully protected by the C layers, against oxidation.

The fitting procedure to determine $\beta$ using Eq. (2) from the transmittance data in the spectral range 62–1300 eV is shown in Fig. 5, for five different photon energies. This procedure has also been implemented and described in detail in earlier work.[33–35,37–39] In the plot of measured transmittance $T$ (on a logarithmic scale) of C/Al/C samples vs Al thickness $d$ at a given photon energy, the data points are fitted to a straight line whose slope is equal to $-4\pi\beta/\lambda$. Furthermore, the point where the straight line intercepts the y-axis is the transmittance $T_0$ at Al thickness $d = 0$, which corresponds to the transmittance of the two C protective layers, whose thickness is the same among all C/Al/C samples. Therefore, at each photon energy, the absorption $\beta$ of Al is obtained from the slope of the straight line and the presence of the C layers is normalized out of the data via the term $T_0$. We emphasize that this method requires the C layer thickness to be the same among all measured samples, as is the case here. The thickness of the Al and C layers in each sample was determined via the GIXR measurements discussed

10 December 2024 22:19:30


© Author(s) 2024

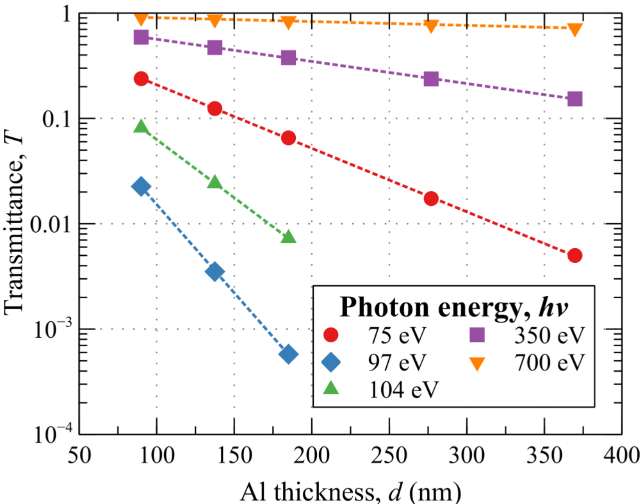


**FIG. 5.** Transmittance (log axis) vs Al thickness (linear axis) for various photon energies. The symbols show the measured transmittance data and the dashed lines represent the fit to the data, according to Eq. (2).

in Sec. III and shown in Table I. It is worth noting that at some photon energies, only three (instead of five) C/Al/C samples were measured and fitted, as is discussed earlier in this section and shown in Fig. 5 (97 and 104 eV). The goodness of each fit was assessed via the value of the coefficient of determination, defined as the square of the Pearson correlation coefficient. This coefficient was higher than 0.997 on the entire spectrum and higher than 0.999 in the Al L edge region (65–175 eV).

To determine the $\delta$ values, which belong to the real part of the refractive index, we used the Kramers–Kronig relation[44] given in the following equation:

$$\delta(E) = -\frac{2}{\pi} P \int_0^{\infty} \frac{E' \beta(E')}{E'^2 - E^2} \, dE, \tag{3}$$

where $P$ denotes the Cauchy principal value of the integral.

The use of Eq. (3) requires values of photoabsorption over a broad energy spectrum. We used the following data to compile a consistent set of photoabsorption coefficient over the entire energy spectrum, from 0.1 meV to 433 keV.

At low energies, from 6.2 meV to 12 eV, we used the data reported by Rakić, which are based on experimental reflectance measurements.[19,21,45] We extended toward lower photon energies by using a Lorentz Drude model down to 0.1 meV.[46] In order to connect the Rakić data with our data and to increase the number of energy values around the Al plasma frequency at 15 eV, we used data from Ref. 45 from 13 to 15 eV and CXRO[13,23] from 15.18 to 16.72 eV. We used the photoabsorption coefficients from this work from 17.2 to 824.2 eV, including values determined by the new methodology described in Ref. 40 from 17.2 to 62 eV and CXRO values from 824.6 to 1493 eV. Note that in the range 824–1300 eV, the present results are in very good agreement with CXRO data (less than 0.6% RMS difference). For the Al K-edge region, from 1.5 to 3 keV, we selected data from Shiles, which have a good spectral resolution at the K edge, including some fine structure.[19] Finally, we used NIST data from 3.5 to 433 keV.[47]

As shown in Fig. 6, this compilation provides continuous values of Al photoabsorption coefficient with an excellent overlap over the entire energy spectrum. Thanks to the good continuity between all sets of data, we did not need to apply any interpolation in-between each set of data. It is interesting to notice that independent measurements by Larruquert *et al.*[18] (not used in this compilation) in the energy range 15–16 eV are in very good agreement with the compilation that we used for the Kramers–Kronig analyses and connect well with our photoabsorption data which start at 17 eV.

We checked that the low- and high-energy limits of this compilation are adequate by verifying that the results obtained with different values for these limits ($10^{-9}$ eV and 331 keV, respectively) were the same.

In addition, we tested the consistency of this compilation by verifying that the f-sum rule for the absorption[33] gives a value close to the theoretical one (12.74 with the present compilation, compared to 12.99 theoretically). This is only 1.9% difference. For comparison, in previous studies, we obtained 1.3% difference for Pt[39] and 4% difference for Cr.[38]

The $\delta$ and $\beta$ values resulting from the present photoabsorption measurements and Kramers–Kronig analyses are plotted in Fig. 7. We have also plotted in Fig. 7 existing data from the literature for comparison: a compilation from Shiles and Palik

10 December 2024 22:19:30

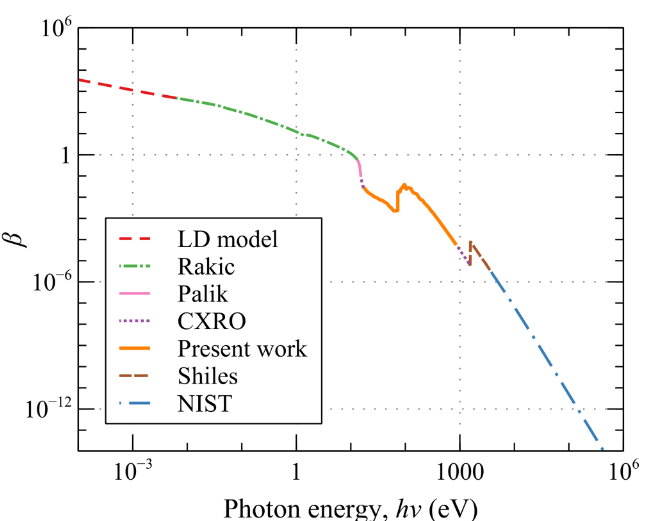


**FIG. 6.** Compilation of $\beta$ values of Al used to calculate $\delta$ according to Eq. (3): Lorentz–Drude model[46] (red dashed line), data based on reflectance measurements from Ref. 21 (green dash-dot line), experimental data from Ref. 45 (pink solid line), tabulated data from Ref. 23 (purple dotted line), experimental data from the present work (orange solid line), experimental data from Ref. 19 (brown dashed line), and tabulated data from Ref. 47 (blue dash-dot line).


© Author(s) 2024

**FIG. 7.** $\delta$ and $\beta$ values from the present work (red solid line) are compared with tabulated data from the literature: compilation[25] of experimental data from Refs. 19 and 45 (blue solid line), tabulated data from Ref. 23 (green solid line), and experimental data from Ref. 20 (cyan diamonds connected by light blue line). The $\delta$ and $\beta$ values are shown in three distinct photon energy ranges: [(a) and (b)] 10–1000 eV (log-log scale), [(c) and (d)] 50–250 eV (log-linear scale), and [(e) and (f)] 72–74 eV (linear scale).

10 December 2024 22:19:30



© Author(s) 2024

(see Ref. 25 for more details),[19,45] current data from CXRO[13,23] and data measured by interferometry around the $L_{2,3}$ -edge.[20]

During an earlier stage of the present work, we have been able to provide more accurate Al photoabsorption ($\beta$) values in the energy range 17–62 eV by using a new method that takes into account the multiple reflections in the Al transmission samples.[40] Note that for energies higher than 50 eV and up to 70 eV, where multiple reflections become negligible, our data are in good agreement with CXRO.

In the energy range 70–300 eV, which includes the Al $L_{2,3}$ edge, our data provide very well-resolved fine structure with features that have not been seen earlier. Differences of up to 30% can be seen between the absorption data in the present work and tabulated (CXRO) values in the region of the Al $L_{2,3}$ edge and up to about 200 eV photon energy. The positions of the main fine structure (peaks and valleys) above 90 eV are consistent with the positions of similar features in Shiles/Palik data.[19,45] Our data provide, however, a more detailed and resolved description of this fine structure. At higher energies, above 300 eV, our $\beta$ values are almost identical to previous CXRO data, within $\pm 1\%$ RMS.

In Fig. 7, the present set of Al $\delta$ values around/below the $L_{2,3}$-edge and up to about 200 eV is markedly different than the tabulated (CXRO) values. Compared with previous independent measurements made by interferometry,[20] the overall agreement in $\delta$ values is remarkable for the abrupt structure of the $L_{2,3}$-edge and up to 80 eV. This constitutes a strong validation of the photoabsorption measurements and Kramers–Kronig analyses performed in this work. The $\beta$ values provided by Ref. 20 appear somewhat scattered below the Al $L_{2,3}$ edge and present an offset with our data just above the edge. This may be due to the fact that only one Al thickness was used for the measurement in Ref. 20, which does not allow to normalize out the effect of sample surface layers. Moreover, as compared to our measurement, the surface of the sample is much smaller ($5 \times 5\,\mu m^2$), which limits the photon flux and the signal-to-noise ratio.

Finally, the present set of Al optical constants has been validated by comparing experimental Al filter transmission with simulations based on Al optical constants from different sources. The experimental data consist of measurements made at PTB/BESSY II facility on Al filter used in a LYRA VUV radiometer.[48] The model contains a 154 nm-thick Al layer with a 4.5 nm-thick amorphous oxide ($Al_2O_3$) on each side. We used optical constants from Hagemann *et al.* for the amorphous $Al_2O_3$ layers.[14] Figure 8 shows that we obtained an excellent agreement between the experimental data and the model when using the present set of Al optical constants, whereas it was not possible to obtain a good agreement on the whole spectral range with previously available Al optical constants.

These results demonstrate that our methodology, combined with Kramers–Kronig analyses using carefully selected photoabsorption data over the entire energy spectrum, provides data with a high signal-to-noise ratio and increased accuracy. The exquisite spectral resolution around the Al $L_{2,3}$ edge is afforded by the exceptional ability to obtain data in steps as small as 0.02 eV at ALS beamline 6.3.2 combined with the high resolving power of the beamline, as discussed in Sec. II D. Detailed, quantitative NEXAFS/XANES information contained in absolute photoabsorption and dispersion data around K, L, M, N, and O edges has also been revealed earlier for several other elements and compounds measured at beamline 6.3.2 (Mo,[33] Be,[34] Y,[35] B4C,[37] B,[36] Cr,[38] and Pt[39]). These data could be used to validate and advance atomic and molecular physics models, such as *ab initio* calculations, that can be found in scientific software and related databases.[49]

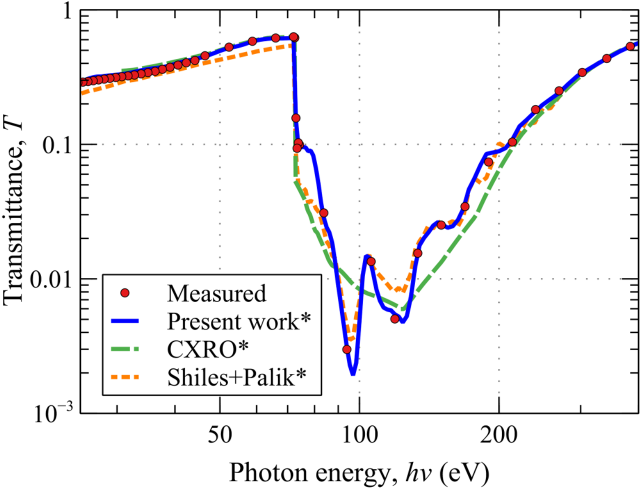


**FIG. 8.** Transmittance measurements and simulations of LYRA Al filter (log-log plot)[48] shown in the 25–400 eV range. The data are shown with red circles, while the solid, dashed, and dotted lines correspond to transmittance simulations (indicated with asterisks in the legend), using optical constants from the present work and values from the literature.[13,19,23,25,45]

## V. CONCLUSIONS

We have determined experimentally a new set of values for the refractive index of aluminum in a wide spectral range, extending from the near-UV to the x-ray region. The Al photoabsorption was measured via transmittance measurements performed on freestanding Al thin films of thicknesses ranging from 45.6 to 369.7 nm, protected against oxidation by 5.5 nm-thick C layers. The samples were characterized via x-ray reflectivity and EUV transmittance, to verify their thickness, density, and purity; they remained stable over a period of 2 years. The Al dispersion was calculated from the photoabsorption data via the Kramers–Kronig transformation. In the Al $L_1$ and $L_{2,3}$ edge spectral regions, the new refractive index values reveal fine structure obtained with step sizes ranging from 0.1 eV down to 0.02 eV; the latter is pushing the limits of what is achievable and was deemed necessary in order to fully resolve the structure right at the $L_{2,3}$ edge. The ability to obtain accurate photoabsorption data in such an extended spectral range with ultrahigh resolution is enabled by the state-of-the-art calibration facility at ALS beamline 6.3.2, as well as by the capability to produce stable, well-characterized freestanding thin films. Such highly resolved experimental data could be valuable toward validating atomic and molecular physics models, such as *ab initio* calculations of band structure. The new set of Al photoabsorption

10 December 2024 22:19:30


© Author(s) 2024

data was validated in the 25–400 eV photon energy range, by modeling the transmittance of an Al-based filter employed aboard a space borne EUV solar radiometer (LYRA). There is remarkable agreement between the new Al data and the measured transmittance of the filter, including in the vicinity of the Al L edges, where previously published values failed to accurately predict the performance. The Al refractive index values from this work will allow the successful design, modeling, and calibration of EUV/x-ray instruments and will be included in the CXRO website, the worldwide reference database for the EUV/x-ray optical properties of materials.

## SUPPLEMENTARY MATERIAL

The file provided as supplementary material corresponds to a compilation of the real part $n = 1 - \delta$ and imaginary part $k = \beta$ of the index of refraction of Al as determined by this work, as a function of wavelength $\lambda$ (in Å units). The header of the file, defined by the first rows that start with a ";" character, contains the list of References to all the data used in the compilation (see also Fig. 6).

## ACKNOWLEDGMENTS

Funding for this work was provided in part by LLNL's Laboratory Directed Research and Development (LDRD) under Project No. 20-FS-026 and CNRS International Research Project "IRP EREUS." This work was performed under the auspices of the U.S. Department of Energy by Lawrence Livermore National Laboratory under Contract No. DE-AC52-07NA27344 and by the University of California Lawrence Berkeley National Laboratory under Contract No. DE-AC03-76F00098, and of the Institut d'Optique Graduate School at Université Paris-Saclay. The authors are thankful to Jeff Robinson (LLNL) for hardware support. Document release number: LLNL-JRNL-867108.

## AUTHOR DECLARATIONS

### Conflict of Interest

The authors have no conflicts to disclose.

### Author Contributions

**Catherine Burcklen:** Data curation (lead); Formal analysis (equal); Funding acquisition (equal); Methodology (equal); Project administration (equal); Validation (equal); Visualization (lead); Writing – original draft (supporting); Writing – review & editing (equal). **Franck Delmotte:** Formal analysis (equal); Funding acquisition (equal); Methodology (equal); Supervision (equal); Validation (equal); Writing – original draft (equal); Writing – review & editing (equal). **Jennifer Alameda:** Investigation (equal). **Farhad Salmassi:** Investigation (equal). **Eric Gullikson:** Investigation (equal); Methodology (equal); Resources (equal); Supervision (supporting). **Regina Soufli:** Formal analysis (equal); Funding acquisition (equal); Investigation (equal); Methodology (equal); Project administration (equal); Supervision (equal); Validation (equal); Writing – original draft (equal); Writing – review & editing (equal).

## DATA AVAILABILITY

The data that support the findings of this study are available within the article and its supplementary material.

## REFERENCES

[1]F. R. Powell, P. W. Vedder, J. F. Lindblom, and S. F. Powell, "Thin film filter performance for extreme ultraviolet and x-ray applications," Opt. Eng. **29**, 614 (1990).
[2]A. J. Corso and M. G. Pelizzo, "Extreme ultraviolet multilayer nanostructures and their application to solar plasma observations: A review," J. Nanosci. Nanotechnol. **19**, 532–545 (2019).
[3]D. L. Windt, "EUV multilayer coatings for solar imaging and spectroscopy," Proc. SPIE **9604**, 96040P (2015).
[4]R. Soufli, M. Fernández-Perea, S. L. Baker, J. C. Robinson, J. Alameda, and C. C. Walton, "Spontaneously intermixed Al-Mg barriers enable corrosion-resistant Mg/SiC multilayer coatings," Appl. Phys. Lett. **101**, 043111 (2012).
[5]M. Fernández-Perea, R. Soufli, J. C. Robinson, L. R. D. Marcos, J. A. Méndez, J. I. Larruquert, and E. M. Gullikson, "Triple-wavelength, narrowband Mg/SiC multilayers with corrosion barriers and high peak reflectance in the 25–80 nm wavelength region," Opt. Express **20**, 24018–24029 (2012).
[6]J. Rebellato, R. Soufli, E. Meltchakov, E. Gullikson, S. de Rossi, and F. Delmotte, "High efficiency Al/Sc-based multilayer coatings in the EUV wavelength range above 40 nm," Opt. Lett. **45**, 869–872 (2020).
[7]J. Rebellato, R. Soufli, E. Meltchakov, E. M. Gullikson, S. de Rossi, C. Baumier, F. Pallier, and F. Delmotte, "Optical, structural and aging properties of Al/Sc-based multilayers for the extreme ultraviolet," Thin Solid Films **735**, 138873 (2021).
[8]E. Meltchakov, C. Hecquet, M. Roulliay, S. De Rossi, Y. Menesguen, A. Jérome, F. Bridou, F. Varniere, M. F. Ravet-Krill, and F. Delmotte, "Development of Al-based multilayer optics for EUV," Appl. Phys. A **98**, 111 (2009).
[9]A. H. K. Mahmoud, S. de Rossi, E. Meltchakov, B. Capitanio, M. Thomasset, M. Vallet, E. Héripré, and F. Delmotte, "Al/Mo/SiC multilayer diffraction gratings with broadband efficiency in the extreme ultraviolet," Opt. Express **30**, 38319–38338 (2022).
[10]A. H. K. Mahmoud, S. de Rossi, E. Meltchakov, B. Capitanio, M. Thomasset, M. Vallet, and F. Delmotte, "Experimental study and modeling of extreme ultraviolet 4000 lines/mm diffraction gratings coated with periodic and aperiodic Al/Mo/SiC multilayers," Appl. Opt. **63**, 30–41 (2024).
[11]F. Delmotte, E. Meltchakov, S. de Rossi, F. Bridou, A. Jérome, F. Varnière, R. Mercier, F. Auchère, X. Zhang, B. Borgo, C. Dumesnil, S. François, M. Roulliay, and U. Strauch, "Development of multilayer coatings for solar orbiter EUV imaging telescopes," Proc. SPIE **8862**, 88620A (2013).
[12]I. Yoshikawa, T. Homma, K. Sakai, G. Murakami, K. Yoshioka, A. Yamazaki, T. Sakanoi, and A. Saito, "Imaging observation of the earth's plasmasphere and ionosphere by EUVI of ISS-IMAP on the international space station," IEEJ Trans. Fundam. Mater. **131**, 1006–1010 (2011).
[13]E. M. Gullikson, P. Denham, S. Mrowka, and J. H. Underwood, "Absolute photoabsorption measurements of Mg, Al, and Si in the soft-x-ray region below the $L_{2,3}$ edges," Phys. Rev. B **49**, 16283–16288 (1994).
[14]H.-J. Hagemann, W. Gudat, and C. Kunz, "Optical constants from the far infrared to the x-ray region: Mg, Al, Cu, Ag, Au, Bi, C, and Al2O3," J. Opt. Soc. Am. **65**, 742–744 (1975).
[15]R. W. Ditchburn and G. H. C. Freeman, "The optical constants of aluminium from 12 to 36 eV," Proc. R. Soc. London, Ser. A **294**, 20–37 (1966).
[16]D. L. Windt, W. C. Cash, M. Scott, P. Arendt, B. Newnam, R. F. Fisher, A. B. Swartzlander, P. Z. Takacs, and J. M. Pinneo, "Optical constants for thin films of C, diamond, Al, Si, and CVD SiC from 24 Å to 1216 Å," Appl. Opt. **27**, 279–295 (1988).
[17]J. I. Larruquert, J. A. Méndez, and J. A. Aznárez, "Far-ultraviolet reflectance measurements and optical constants of unoxidized aluminum films," Appl. Opt. **34**, 4892–4899 (1995).

10 December 2024 22:19:30


© Author(s) 2024

[18]J. I. Larruquert, J. A. Méndez, and J. A. Aznárez, "Optical constants of aluminum films in the extreme ultraviolet interval of 82–77 nm," Appl. Opt. **35**, 5692–5697 (1996).
[19]E. Shiles, T. Sasaki, M. Inokuti, and D. Y. Smith, "Self-consistency and sum-rule tests in the Kramers-Kronig analysis of optical data: Applications to aluminum," Phys. Rev. B **22**, 1612–1628 (1980).
[20]C. Chang, E. Anderson, P. Naulleau, E. Gullikson, K. Goldberg, and D. Attwood, "Direct measurement of index of refraction in the extreme-ultraviolet wavelength region with a novel interferometer," Opt. Lett. **27**, 1028–1030 (2002).
[21]A. D. Rakić, "Algorithm for the determination of intrinsic optical constants of metal films: Application to aluminum," Appl. Opt. **34**, 4755–4767 (1995).
[22]B. Henke, E. Gullikson, and J. Davis, "X-ray interactions: Photoabsorption, scattering, transmission, and reflection at E = 50–30 000 eV, Z = 1–92," At. Data Nucl. Data Tables **54**, 181–342 (1993).
[23]See http://henke.lbl.gov/optical_constants/ for an updated version of Ref. 22.
[24]P. Boerner, C. Edwards, J. Lemen, A. Rausch, C. Schrijver, R. Shine, L. Shing, R. Stern, T. Tarbell, A. Title, C. J. Wolfson, R. Soufli, E. Spiller, E. Gullikson, D. McKenzie, D. Windt, L. Golub, W. Podgorski, P. Testa, and M. Weber, "Initial calibration of the atmospheric imaging assembly (AIA) on the solar dynamics observatory (SDO)," Sol. Phys. **275**, 41–66 (2012).
[25]J. Rebellato, E. Meltchakov, R. Soufli, S. D. Rossi, X. Zhang, F. Auchère, and F. Delmotte, "Analyses of tabulated optical constants for thin films in the EUV range and application to solar physics multilayer coatings," Proc. SPIE **10691**, 106911U (2018).
[26]R. Soufli and E. M. Gullikson, "Reflectance measurements on clean surfaces for the determination of optical constants of silicon in the extreme ultraviolet–soft-x-ray region," Appl. Opt. **36**, 5499–5507 (1997).
[27]Q. Saadeh, P. Naujok, D. Thakare, M. Wu, V. Philipsen, F. Scholze, C. Buchholz, Z. Salami, Y. Abdulhadi, D. O. García, H. Mentzel, A. Babuschkin, C. Laubis, and V. Soltwisch, "On the optical constants of cobalt in the M-absorption edge region," Optik **273**, 170455 (2023).
[28]R. Ciesielski, Q. Saadeh, V. Philipsen, K. Opsomer, J.-P. Soulié, M. Wu, P. Naujok, R. W. E. van de Kruijs, C. Detavernier, M. Kolbe, F. Scholze, and V. Soltwisch, "Determination of optical constants of thin films in the EUV," Appl. Opt. **61**, 2060–2078 (2022).
[29]C. Tarrio, R. N. Watts, T. B. Lucatorto, J. M. Slaughter, and C. M. Falco, "Optical constants of in situ-deposited films of important extreme-ultraviolet multilayer mirror materials," Appl. Opt. **37**, 4100–4104 (1998).
[30]R. Soufli and E. M. Gullikson, "Optical constants of materials for multilayer mirror applications in the EUV/soft x-ray region," Proc. SPIE **3113**, 222–229 (1997).
[31]W. R. Hunter, "Measurement of optical properties of materials in the vacuum ultraviolet spectral region," Appl. Opt. **21**, 2103–2114 (1982).
[32]D. Attwood and A. Sakdinawat, *X-Rays and Extreme Ultraviolet Radiation: Principles and Applications*, 2nd ed. (Cambridge University Press, 2017),
[33]R. Soufli and E. M. Gullikson, "Absolute photoabsorption measurements of molybdenum in the range 60–930 eV for optical constant determination," Appl. Opt. **37**, 1713–1719 (1998).
[34]R. Soufli, S. Bajt, and E. M. Gullikson, "Optical constants of beryllium from photoabsorption measurements for x-ray optics applications," Proc. SPIE **3767**, 251–258 (1999).
[35]B. Sae-Lao and R. Soufli, "Measurements of the refractive index of yttrium in the 50–1300 eV energy region," Appl. Opt. **41**, 7309–7316 (2002).
[36]M. Fernández-Perea, J. I. Larruquert, J. A. Aznárez, J. A. Méndez, M. Vidal-Dasilva, E. Gullikson, A. Aquila, R. Soufli, and J. L. G. Fierro, "Optical constants of electron-beam evaporated boron films in the 6.8–900 eV photon energy range," J. Opt. Soc. Am. A **24**, 3800–3807 (2007).
[37]R. Soufli, A. L. Aquila, F. Salmassi, M. Fernández-Perea, and E. M. Gullikson, "Optical constants of magnetron-sputtered boron carbide thin films from photoabsorption data in the range 30 to 770 eV," Appl. Opt. **47**, 4633–4639 (2008).
[38]F. Delmotte, J. Meyer-Ilse, F. Salmassi, R. Soufli, C. Burcklen, J. Rebellato, A. Jérome, I. Vickridge, E. Briand, and E. Gullikson, "Soft x-ray optical constants of sputtered chromium thin films with improved accuracy in the L and M absorption edge regions," J. Appl. Phys. **124**, 035107 (2018).
[39]R. Soufli, F. Delmotte, J. Meyer-Ilse, F. Salmassi, N. Brejnholt, S. Massahi, D. Girou, F. Christensen, and E. M. Gullikson, "Optical constants of magnetron sputtered Pt thin films with improved accuracy in the N- and O-electronic shell absorption regions," J. Appl. Phys. **125**, 085106 (2019).
[40]F. Delmotte, C. Burcklen, J. Alameda, F. Salmassi, E. Gullikson, and R. Soufli, "New method for the determination of photoabsorption from transmittance measurements in the extreme ultraviolet," Opt. Express **30**, 23771–23782 (2022).
[41]J. Underwood and E. Gullikson, "High-resolution, high-flux, user friendly VLS beamline at the ALS for the 50–1300 eV energy region," J. Electron Spectrosc. Relat. Phenom. **92**, 265–272 (1998).
[42]E. M. Gullikson, S. Mrowka, and B. B. Kaufmann, "Recent developments in EUV reflectometry at the advanced light source," Proc. SPIE **4343**, 363–373 (2001).
[43]See https://cxro.lbl.gov/als632/index.php?content=res.html for information about beamline 6.3.2 spectral resolving power vs photon energy for various monochromator gratings.
[44]M. Altarelli, D. L. Dexter, H. M. Nussenzveig, and D. Y. Smith, "Superconvergence and sum rules for the optical constants," Phys. Rev. B **6**, 4502–4509 (1972).
[45]D. Smith, E. Shiles, and M. Inokuti, "The optical properties of metallic aluminum," in *Handbook of Optical Constants of Solids*, edited by E. D. Palik (Academic Press, Burlington, 1997), pp. 369–406.
[46]A. D. Rakić, A. B. Djurišić, J. M. Elazar, and M. L. Majewski, "Optical properties of metallic films for vertical-cavity optoelectronic devices," Appl. Opt. **37**, 5271–5283 (1998).
[47]C. T. Chantler, "Theoretical form factor, attenuation, and scattering tabulation for Z = 1–92 from E = 1–10 eV to E = 0.4–1.0 MeV," J. Phys. Chem. Ref. Data **24**, 71–643 (1995).
[48]M. Dominique, J. F. Hochedez, W. Schmutz, I. E. Dammasch, A. I. Shapiro, M. Kretzschmar, A. N. Zhukov, D. Gillotay, Y. Stockman, and A. BenMoussa, "The LYRA instrument onboard PROBA2: Description and in-flight performance," Sol. Phys. **286**, 21–42 (2013).
[49]Y. Chen, C. Chen, C. Zheng, S. Dwaraknath, M. K. Horton, J. Cabana, J. Rehr, J. Vinson, A. Dozier, J. J. Kas, K. A. Persson, and S. P. Ong, "Database of ab initio L-edge x-ray absorption near edge structure," Sci. Data **8**, 153 (2021).

10 December 2024 22:19:30


© Author(s) 2024